

NEAR-FIELD 3-D SYNTHETIC APERTURE RADAR IMAGING VIA COMPRESSED SENSING

Zengli Yang and Yahong Rosa Zheng

Department of Electrical & Computer Engineering
Missouri University of Science and Technology
(formerly University of Missouri-Rolla)
Rolla, MO, 65409, USA

ABSTRACT

This paper successfully implements compressed sensing (CS) to a near-field wideband 3-D synthetic aperture radar (SAR) imaging system. SAR data are measured at a low percentage of random-selected positions on a uniform grid of planar aperture in the stripmap mode. The near-field 3-D range migration algorithm (RMA) is used in combination with the CS principle to reconstruct the 3-D image via l_1 regularized least-square approach. Experiments were performed with Q-band stepped-frequency monostatic stripmap SAR imaging system on a blue foam embedded with eight rubber pads and one copper square chip. The results of the experiments show near-field 3-D image of the specimen under test (SUT) can be reconstructed efficiently from low percentage of the full measurement positions, which largely lessens the data collection load. The reconstructed image was better focused and denoised.

Index Terms— Near-field, 3-D radar imaging, compressed sensing (CS), synthetic aperture radar (SAR), nondestructive testing and evaluation (NDT&E).

1. INTRODUCTION

Near-field synthetic aperture radar (SAR) imaging finds important applications in the area of nondestructive testing and evaluation (NDT&E) [1] for its feasibility to acquire high-resolution holographic images of specimen under test (SUT). Microwave and millimeter wave NDT&E techniques have been applied to diverse applications, such as detection and evaluation of corrosion under paint and composite laminates, fatigue crack detection and sizing in metal surfaces, dielectric material characterization, etc.

However, data collection for near-field 3-D SAR imaging imposes great challenges on wideband application of these 3-D imaging system. Conventional raster scanning usually takes several hours to scan a $2'$ by $2'$ area. Compressed sensing (CS) theory delivers an idea of transferring the load of

signal acquisition to signal reconstruction, which indicates its potential applications in near-field 3-D SAR imaging. For remote sensing with radar, the application of CS has been surveyed extensively in [2], where fewer 3-D Fourier (k -space) measurements are obtained at the airborne radar from multiple elevation passes.

Unlike far-field SAR imaging, a spherical wave cannot be approximated by a plane wave in near-field situation. Achieving complete wavefront curvature correction, the range migration algorithm (RMA) is considered as the more appropriate near-field 3-D SAR imaging algorithm [3]. Also, near-field 3-D reflectivity image is usually formed by synthesizing a 2-D planar aperture with a wideband radar. Compared with the polar format algorithm (PFA), near-field 3-D RMA requires additional 2-D cross-range Fourier transform and 1-D Stolt interpolation [4] to acquire the k -space data. The major drawback of RMA comes from the inaccurate Stolt interpolation, which results in shading and multiple mirror images of the interrogated scene [5]. For sparse 3-D near-field imaging, it is practical to perform 2-D pseudorandom sampling with uniform density on the 2-D aperture plane to extract the features of SUT in 3-D Cartesian space exhaustively and decrease the load of data collection simultaneously. With randomness of the measurements, the major drawback of RMA can be mitigated in CS reconstruction by enforcing the sparsity of the 3-D image of SUT.

The previous method [6], based on nonuniform fast Fourier transform (NUFFT) and seeking sparse domains for the measurements, failed to converge for wideband 3-D SAR representation using CS. In this paper, we propose a new rigorous approach of near-field 3-D SAR imaging via CS based on Stolt interpolation, and investigate the influence of CS on the quality of reconstructed images. The experimental data was collected by the wideband, monostatic, stepped-frequency, stripmap SAR imaging system developed at Missouri S&T. According to the *a priori* information of SUT, suitable sparse domain of the reflectivity image was chosen to demonstrate the performance of our near-field sparse 3-D SAR imaging approach.

This work was supported by the University of Missouri Research Board fund.

2. COMPRESSED SENSING FOR 3-D RADAR IMAGING

In radar imaging, compressed sensing methodology can retrieve the interrogated scene from fewer measurements without losing much information [7]. Briefly, the basic idea for far-field imaging via CS can be interpreted as

$$\min_{\mathbf{x}} \|\mathbf{x}\|_1 \quad \text{subject to} \quad \Phi \mathbf{g} = \mathbf{r}, \quad \Psi \mathbf{g} = \mathbf{x}, \quad (1)$$

where $\|\cdot\|_1$ denotes l_1 -norm, $\mathbf{g} \in \mathbb{C}^{n \times 1}$ is the reflectivity of the interrogated scene, $\Psi \in \mathbb{C}^{n \times n}$ is the linear operator that transforms from voxel representation into a sparse representation, and $\mathbf{x} \in \mathbb{C}^{n \times 1}$ is the sparse representation of scene's reflectivity \mathbf{g} . Also, $\Phi \in \mathbb{C}^{m \times n}$ ($m < n$) is the measurement matrix, which reflects the acquisition of limited vectorized received measurements $\mathbf{r} \in \mathbb{C}^{m \times 1}$ for the scene's reflectivity.

To ensure the solution of (1), Φ and Ψ are to satisfy the restricted isometry property (RIP) which is verified by mutual coherence [8] calculated as $\mu = \max_{j \neq k} |\langle \phi_j, \psi_k \rangle|$ where ϕ_j is the j^{th} column of Φ , and ψ_k is the k^{th} row of Ψ . The coherence measures the largest correlation between any two elements of Φ and Ψ , and lower coherence pairs help remove the incoherent artifacts caused by sub-Nyquist sampling. Random measurement matrix for Φ is preferred owing to its large incoherence with any fixed basis for Ψ .

3. NEAR-FIELD 3-D SAR IMAGING VIA COMPRESSED SENSING

3.1. Near-Field 3-D SAR Imaging

Consider a near-field monostatic stripmap 3-D SAR imaging system where data is collected by scanning the SUT over a 2-D planar aperture denoted as XY -plane. A point target is characterized by its reflectivity function $g(x', y', z')$. In 3-D Cartesian space, we assume the dimension perpendicular to the 2-D aperture plane as the Z -dimension and its origin is located at the 2-D aperture plane. With near-field assumption, the wavefront curvature is no longer negligible. Without performing plane wave approximation for spherical wave, the received spherical waveform at position (x, y) with temporal angular frequency ω is given by

$$r(x, y, \omega) = \iint \int g(x', y', z') \times e^{-j2k\sqrt{(x-x')^2 + (y-y')^2 + z'^2}} dx' dy' dz' \quad (2)$$

where $\omega = 2\pi f$ with f being temporal frequency, $k = \omega/c$ is the wavenumber with c being the propagation speed of light, and $g(x', y', z')$ denotes the 3-D reflectivity function of SUT. With plane wave decomposition for spherical wave, Fourier transform and Stolt interpolation, the 3-D reflectivity function of the SUT is give by [3] [9]

$$g(x, y, z) = \mathcal{F}_{3D}^{-1} \{ \Theta \{ \mathcal{F}_{2D} [r(x, y, \omega)] e^{-jk_z z} \} \} \quad (3)$$

where \mathcal{F}_{2D} denotes 2-D fast Fourier transform (FFT), \mathcal{F}_{3D}^{-1} denotes 3-D inverse FFT (IFFT), and Θ denotes Stolt interpolator. Note that the distinction between the primed and unprimed coordinate systems is now dropped because the coordinate systems coincide after the FFT and IFFT.

Let $P(k_x, k_y, k)$ represent the 2-D cross-range Fourier transform of $r(x, y, \omega)$ and $G(k_x, k_y, k_z)$ represent the 3-D Fourier transform of the reflectivity function $g(x, y, z)$, where k_x, k_y , and k_z are the wavenumbers in the x, y , and z dimensions, respectively, then $k_z = \sqrt{4k^2 - k_x^2 - k_y^2}$ in radar wave propagation. Note that among the three traditional SAR imaging algorithms (PFA, RMA, chirp scaling algorithm (CSA)), only RMA is eligible for near-field 3-D SAR imaging without distortion thanks to its unique capability of correcting wavefront curvature completely. Under uniform measurement grid, Stolt interpolation needs to obtain equispaced $G(k_x, k_y, k_z)$ for 3-D IFFT operation. Alternatively, nonuniform spaced $G(k_x, k_y, k_z)$ can be transformed to the reflectivity image by applying NUFFT [6]. In this paper, we adopt the Stolt transform approach for its low computational complexity. The complete image reconstruction procedure is summarized as shown in Fig. 1.

3.2. Proposed CS Approach for Near-Field 3-D SAR Imaging

To take the advantage of compressed sensing for near-field 3-D SAR imaging, we are to design random and sparse measurement matrix Φ to lessen the workload of data collection. We place radar probe at a small percentage of randomly-selected positions on the uniform XY grid. The backscatter data at these positions are collected and saved as the raw data vector \mathbf{r} . Let \mathbf{U} denotes the binary matrix, which is to select estimated received waveform at these random positions. According to (3), we write the measurement operator Φ as

$$\Phi = \mathbf{U} \mathcal{F}_{2D}^{-1} \{ \Theta^{-1} \{ [\mathcal{F}_{3D}(\cdot)] e^{jk_z z} \} \} \quad (4)$$

where Θ^{-1} is the inverse Stolt interpolator.

In near-field imaging, the sparse domain of the reflectivity image largely depends on the type of SUT. Point scattering objects like corrosion under paint are sparse in the identity domain, and smooth geometrical structures like rebar inside the concrete may be sparse in the Fourier or wavelet domain. Near-optimal sparse transform matrix Ψ will be selected appropriately according to the *a priori* information of SUT.

For CS iterative reconstruction, we formulate (1) as the l_1 regularized least-squares problem,

$$\hat{\mathbf{g}} = \arg \min_{\mathbf{g}} \|\Phi \mathbf{g} - \mathbf{r}\|_2^2 + \lambda_1 \|\Psi \mathbf{g}\|_1 + \lambda_2 TV_{3D}(\mathbf{g}) \quad (5)$$

where $\hat{\mathbf{g}}$ is the estimated reflectivity image, Φ is defined in (4), \mathbf{r} is the vectorized incomplete SAR measurements, and TV_{3D} represents discrete 3-D total variation (TV)-norm derived from [10]. Here, TV-norm is used to force the finite

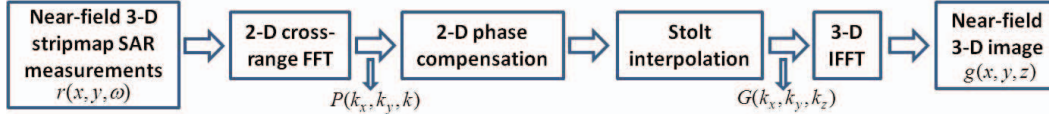


Fig. 1. Simplified block diagram for near-field 3-D range migration algorithm (RMA).

difference of SUT's 3-D image. Especially for RMA in near-field 3-D imaging, TV-norm is necessary for removing the shadow and artifacts in the reflectivity image caused by inaccurate Stolt interpolation. Moreover, λ_1 and λ_2 are the regularization parameters that determine the trade-off among measurement consistency, sparsity in Ψ domain and finite difference domain, respectively.

To solve (5) efficiently, nonlinear conjugate gradient (CG) descent algorithm with backtracking line search [11] is adopted. The gradient of the l_1 -norm was approximated by using the relaxation of the absolute value $|u| = \sqrt{u^*u + \epsilon}$, where $*$ denotes conjugate operator and ϵ is a positive smoothing parameter.

4. EXPERIMENT AND RESULTS

The experiment was performed on the near-filed monostatic stripmap SAR imaging system at the Applied Microwave Nondestructive Testing Laboratory (*amntl*) at Missouri S&T as shown in Fig. 2. Using a wideband stepped-frequency radar, a 2-D planar aperture was synthesized to receive the backscatter data in the frequency band. One set of near-field SAR measurement, blue foam data, was used to evaluate the proposed CS based near-field 3-D SAR imaging.



Fig. 2. Near-field monostatic stripmap SAR imaging system at Missouri S&T.

The blue foam data was collected for the SUT composed of eight rubber patches and one copper patch placed on the above of the blue foam. The standoff distance of the horn antenna is 32 mm, and the scanning area is about $180 \times 120 \text{ mm}^2$. The sampling interval in the XY -plane is 2 mm in both X and Y directions, and the stepped-frequencies is ranged from 35.04 GHz to 44.64 GHz in the Q-band with a step-size

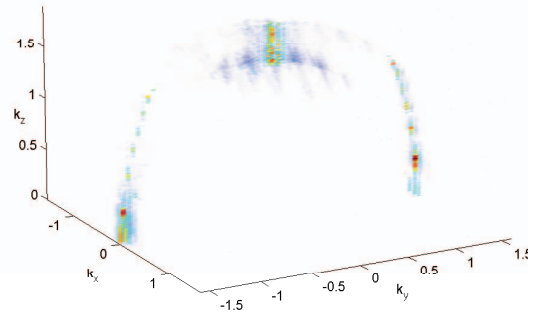


Fig. 3. Magnitude of the 3-D k -space coefficients of the blue foam data.

of 0.64 GHz. The full set of the blue foam measurements is a $91 \times 61 \times 16$ complex data cube corresponding to $r(x, y, \omega)$. Using 3-D RMA directly, the magnitude of the k -space coefficients $G(k_x, k_y, k_z)$ is shown in Fig. 3. Also, Fig. 4 shows the recovered wideband 3-D image for the full set of blue foam data, which indicates the specific positions of the nine patches. As a result of power loss in the propagation path of electromagnetic wave, the upper patches show higher contrast than the lower patches. Besides the environment noise, the shadow of the patches and blue foam is also noticeable, which is caused by the inaccuracy of Stolt interpolation.

For the blue foam benchmark, we randomly select 35% of the XY positions for the scanning area. Fig. 5 shows the reconstructed 3-D images of the nine patches CS. In solving (5), more emphasis was put on enforcing the sparsity in the identity domain ($\lambda_1 = 0.3$) instead of finite difference domain ($\lambda_2 = 0.2$). Comparing to Fig. 4, the shadow and artifacts were removed completely, and nine patches were highlighted with high signal-to-noise ration (SNR). By enforcing the sparsity in the objective function of CS model, the reconstructed 3-D image of the blue foam benchmark can keep the resolution unchanged even for sub-Nyquist sampling.

The CS reconstruction was performed in MATLAB R2010a (x64) on system with the processor Intel(R) Core(TM)2 Quad CPU Q9400 @ 2.66Hz 2.67 GHz and 8.00 GB RAM. Since the maximum range $R_{\max} = c/(4\delta_f)$ with δ_f being the frequency interval, $R_{\max} \approx 117 \text{ mm}$ for the blue foam benchmark. We set the sampling interval along the Z -dimension $\delta_z = 1.667$, so the data cube of the 3-D image had

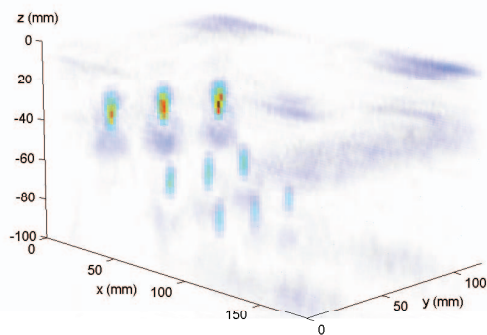


Fig. 4. Wideband 3-D image recovered from the full set of blue foam data directly.

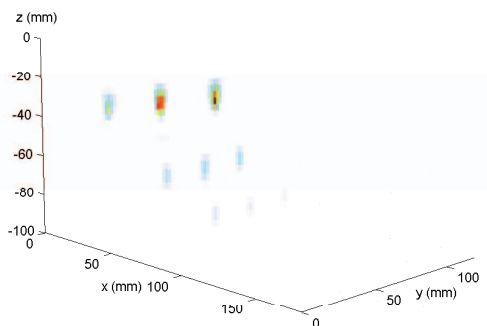


Fig. 5. Wideband 3-D images reconstructed from 35% of the full blue foam data via CS. $\lambda_1 = 0.3$, $\lambda_2 = 0.2$, $\Psi = \mathbf{I}$.

the dimension of $91 \times 61 \times 70$. It took 40 seconds with 15 CG iterations to reconstruct the 3-D image shown in Fig. 5. With 35% undersampling rate, the data collection time was reduced significantly from 40 minutes to 14 minutes.

5. CONCLUSION

A compressed sensing (CS) technique has been successfully implemented in a near-field wideband 3-D SAR imaging system. By measuring only low percentage of the spatial positions randomly selected from uniform grid on a planar aperture, the 3-D image is reconstructed efficiently by CS via l_1 regularized least-squares approach with enhanced quality in terms of more focused targets and reduced noise. The CS reconstruction via a PC is fast with negligible time compared with data scanning time.

6. ACKNOWLEDGEMENT

We wish to thank Dr. Reza Zoughi for providing the experimental data of near-field SAR and Mr. Hamed Kajbaf and Mr. Toby Case for helpful discussion on the RMA and NUFFT algorithms.

7. REFERENCES

- [1] S. Kharkovsky and R. Zoughi, "Microwave and millimeter wave nondestructive testing and evaluation - overview and recent advances," *IEEE Instrum. Meas. Mag.*, vol. 10, no. 2, pp. 26–38, Apr. 2007.
- [2] L. C. Potter, E. Ertin, J. T. Parker, and M. Cetin, "Sparsity and compressed sensing in radar imaging," *Proc. IEEE*, vol. 98, no. 6, pp. 1006–1020, Jun. 2010.
- [3] J. M. Lopez-Sanchez and J. Fortuny-Guasch, "3-D radar imaging using range migration techniques," *IEEE Trans. Antennas Propagat.*, vol. 48, no. 5, pp. 728–737, May 2000.
- [4] R. H. Stolt, "Migration by Fourier transform," *Geophysics*, vol. 43, no. 1, pp. 23–48, 1978.
- [5] R. Bamler, "A comparison of range-Doppler and wavenumber domain SAR focusing algorithms," *IEEE Trans. Geosci. Remote Sens.*, vol. 30, no. 4, pp. 706–713, Jul. 1992.
- [6] H. Kajbaf, J. T. Case, and Y. R. Zheng, "3D image reconstruction from sparse measurement of wideband millimeter wave SAR experiments," in *IEEE Int'l Conf. Image Processing (ICIP2011)*, Sep 2011. In Press.
- [7] R. Baraniuk and P. Steeghs, "Compressive radar imaging," in *IEEE Radar Conf. (Radar'07)*, Apr. 2007, pp. 128–133.
- [8] E. J. Candes and M. B. Wakin, "An introduction to compressive sampling," *IEEE Signal Process. Mag.*, vol. 25, no. 2, pp. 21–30, Mar. 2008.
- [9] D. M. Sheen, D. L. McMakin, and T. E. Hall, "Three-dimensional millimeter-wave imaging for concealed weapon detection," *IEEE Trans. Microwave Theory Tech.*, vol. 49, no. 9, pp. 1581–1592, Sep. 2001.
- [10] A. Chambolle, "An algorithm for total variation minimization and applications," *J. Math. Imaging Vision*, vol. 20, pp. 89–97, 2004.
- [11] M. Lustig, D. Donoho, and J. M. Pauly, "Sparse MRI: The application of compressed sensing for rapid MR imaging," *Magn Reson. Med.*, vol. 58, no. 6, pp. 1182–1195, 2007.